Materials Horizons

ROYAL SOCIETY OF CHEMISTRY

COMMUNICATION

View Article Online
View Journal | View Issue

Cite this: *Mater. Horiz.*, 2025, **12**, 5917

Received 18th April 2025,
Accepted 14th May 2025

DOI: 10.1039/d5mh00735f

rsc.li/materials-horizons

Molecular engineering of donor–acceptor-type conjugated microporous polymers for dual effective photocatalytic production of hydrogen and hydrogen peroxide†

Mohamed Gamal Mohamed, ‡*[ab] Islam M. A. Mekhemer,‡[bc] Ahmed F. H. Selim,‡[bc] Andreas Katsamitros,[d] Dimitrios Tasis,*[de] Abdul Basit,[a] Ho-Hsiu Chou *[cfgh] and Shiao-Wei Kuo *[ai]

Conjugated microporous polymers (CMPs) have garnered increasing attention as emerging polymeric photocatalysts for solar-driven hydrogen (H_2) and hydrogen peroxide (H_2O_2) production, owing to their high surface areas, extended π-conjugation, and tunable architectures. In pursuit of this goal, we undertook the rational design and synthesis of two donor–acceptor CMPs, PyPh-DBZS and ANTh-DBZS, *via* Suzuki coupling polymerization. These CMPs integrate electron-rich pyrene (PyPh) or tetrathienoanthracene (ANTh) donor units with the electron-deficient benzothiophene *S*,*S*-dioxide (DBZS) acceptor moiety, enabling efficient dual photocatalytic generation of H_2 and H_2O_2. Notably, both polymers exhibit excellent thermal stability with T_{10} values exceeding 590 °C and high char yields at 800 °C. PyPh-DBZS CMP exhibited an exceptional H_2 evolution rate (HER) of 133 241 μmol g^{-1} h^{-1}. At the same time, ANTh-DBZS CMP achieved superior H_2O_2 production (24.51 mM g^{-1}), demonstrating structure-dependent charge separation under visible light irradiation. These results offer critical design principles for the rational emergence of new-generation CMPs photocatalysts, paving the way toward efficient and sustainable H_2 and H_2O_2 production.

New concepts

This work tackles a pressing environmental issue by designing innovative, low-cost, and eco-friendly conjugated microporous polymer (CMP)-based semiconductor photocatalysts—namely PyPh-DBZS and ANTh-DBZS CMPs—for harnessing solar energy to produce hydrogen (H_2) and hydrogen peroxide (H_2O_2). These polymers are particularly suited for this dual-function photocatalysis due to their good surface areas, extended π-electron systems, and structural tunability. In our design, we strategically couple electron-rich donor motifs—pyrene (Py) or tetrathienoanthracene (ANTh)—with an electron-deficient acceptor unit, benzothiophene *S*,*S*-dioxide (DBZS), to construct donor–acceptor-type CMPs that facilitate efficient light-induced charge separation. Remarkably, both polymers show outstanding thermal robustness, with decomposition temperatures ($T_{d_{10}}$) surpassing 590 °C and high carbon residue retention at 800 °C. Among the synthesized materials, PyPh-DBZS CMP demonstrated an impressive hydrogen evolution rate (HER) of 133 241 μmol g^{-1} h^{-1}, whereas ANTh-DBZS CMP excelled in hydrogen peroxide production, reaching 24.51 mM g^{-1}. These performance metrics underscore the pivotal role of molecular architecture in dictating charge carrier dynamics and photocatalytic behavior under visible light. Altogether, our findings highlight a powerful strategy for designing next-generation CMP photocatalysts with dual-functional output, offering a blueprint for advancing sustainable and efficient solar-to-chemical energy conversion systems.

1. Introduction

Semiconductor-based photocatalytic processes in aqueous environments have been considered a promising strategy toward the generation of high added value adducts and have been strongly correlated with environmental issues.[1–3] A large variety of reductive/oxidative paths may give rise to various

[a] *Department of Materials and Optoelectronic Science, Center for Functional Polymers and Supramolecular Materials, National Sun Yat-Sen University, Kaohsiung 804, Taiwan. E-mail: kuosw@faculty.nsysu.edu.tw*
[b] *Department of Chemistry, Faculty of Science, Assiut University, Assiut 71515, Egypt. E-mail: mgaml.eldin12@aun.edu.eg, mgamal.eldin12@yahoo.com*
[c] *Department of Chemical Engineering, National Tsing Hua University, Hsinchu 300044, Taiwan. E-mail: hhchou@mx.nthu.edu.tw*
[d] *Department of Chemistry, University of Ioannina, 45110 Ioannina, Greece. E-mail: dtassis@uoi.gr*
[e] *Institute of Materials Science and Computing, University Research Center of Ioannina (URCI), Ioannina 45110, Greece*
[f] *Institute of Photonics Technologies, National Tsing Hua University, Hsinchu 30013, Taiwan*
[g] *College of Semiconductor Research, National Tsing Hua University, Hsinchu 300044, Taiwan*
[h] *Photonics Research Center, National Tsing Hua University, Hsinchu 300044, Taiwan*
[i] *Department of Medicinal and Applied Chemistry, Kaohsiung Medical University, Kaohsiung 807, Taiwan*
† Electronic supplementary information (ESI) available. See DOI: https://doi.org/10.1039/d5mh00735f
‡ These authors contributed equally to this work.

photocatalytic applications. The photoexcited electrons occupying the conduction band may participate in reductive half-reactions, whereas the holes occupying the valence band may act as oxidation agents. Such redox processes include the reductive conversion of greenhouse gases (*e.g.* CO_2) to methane, nitrogen fixation, oxidative water-driven hydrogen fuel production, pollutant degradation, hydrogen peroxide evolution, and so on.[4] The photocatalytic performances are strongly influenced by the light absorption behavior and charge transport efficiency of the photocatalytic materials. The latter process may be highly facilitated through the development of heterojunctions.[5] Furthermore, it is of high importance to develop multifunctional catalysts that exhibit enhanced performance in multiple photoinduced chemical transformations. Besides the well-studied inorganic semiconductors, carbon-based semiconducting species have been developed throughout the recent decades, involving either graphitic allotropes,[6] porous organic frameworks, and acquiring variable crystallinity.[7] Within the latter family, the so-called conjugated microporous polymers (CMPs) are considered as porous networks with rather amorphous character, originating through crosslinking reactions of properly end-functionalized monomer units. Various organic chemistry schemes have been adopted to construct microporous networks consisting of conjugated structural units.[8–16] In the seminal work of Cooper and co-workers,[17] poly(aryleneethynylene) networks were constructed employing the Sonogashira–Hagihara coupling approach between tri-alkyne- and di-halogen-modified arenes.

In the following years, great advances have been accomplished in the synthesis of analogous conjugated networks, and their applications have been described in excellent review articles.[13,18] By tuning the spatial combination of conjugated monomers in either 2D or 3D fashion, one may develop a built-in electric field through the backbone of the network for optimization of charge transfer phenomena. To this end, CMP-based systems have been studied as efficient photocatalysts for hydrogen generation,[19] pollutant degradation,[20] CO_2 reduction,[21] and H_2O_2 evolution,[22] with the latter photo process being the least studied in comparison. Besides hydrogen gas, an environmentally friendly fuel, hydrogen peroxide (H_2O_2) has recently received much interest due to its potential applicability as a green oxidant in the paper industry as well as a high-energy density component in rocket propulsion systems. The most utilized synthetic protocol is the so-called anthraquinone process, which has high energy demands and produces harmful by-products. Thus, tremendous efforts have taken place in order to develop photocatalytic systems with enhanced H_2O_2 evolution rates. Formation of the peroxide may be achieved by either two-electron oxygen reduction or two-hole water oxidation in an aqueous environment.[23] The spatial separation of redox catalytic sites, combined with the porous character of CMPs, makes these materials an ideal platform for achieving efficient performance in multiple photo processes. Regarding the selection of proper conjugated units, dibenzothiophene dioxide derivatives have been integrated into donor–acceptor-geometry CMPs, leading to enhanced photocatalytic performance. A variety of monomer units have been compounded with the above-mentioned chromophore, such as phenylene sequences,[24] pyrene,[25–28] spirobifluorene,[29] dibenzochrysene,[30] triazine,[31,32] triphenylamine,[33] biphenothiazine,[34] and triindole.[35] All the aforementioned studies were focused on the photocatalytic hydrogen evolution reaction. It is noted that, in certain cases, further enhancement in photocatalytic performance was achieved by decoration of noble metal cocatalysts, such as Pt. In far less studied photo processes, analogous dibenzothiophene dioxide-based CMPs have been studied as potential photocatalysts for uranium reduction.[36] In general, the development of dual-function CMP systems has not been demonstrated in the related literature. To our knowledge, there have been a couple of works studying CMP systems in either simultaneous or separate photocatalytic processes. The groups of Ouyang,[37] and Gu[38] have independently studied the simultaneous H_2O_2 evolution accompanied by pollutant degradation. It is well known that both reductive and oxidative reactions in an aerated aqueous environment produce the so-called reactive oxygen species (ROS) family, in which hydrogen peroxide belongs, along with other transient intermediates. Alternatively, dual-function photocatalysis may be demonstrated in separate photocatalytic reactions, which take place in different atmospheric conditions. To address the concerns mentioned above, two donor–acceptor CMPs, PyPh-DBZS and ANTh-DBZS CMPs, were synthesized by Suzuki polymerization for photocatalytic applications by integrating PyPh or ANTh with DBZS. PyPh-DBZS CMP exhibited an HER of 133 241 μmol g^{-1} h^{-1} under visible light, surpassing ANTh-DBZS CMP (34 791 μmol μmol g^{-1} h^{-1}) due to enhanced charge separation. Moreover, ANTh-DBZS CMP demonstrated superior H_2O_2 production (24.51 mM g^{-1}, 3 h) relative to PyPh-DBZS CMP (4.76 mM g^{-1}), highlighting structure-dependent photocatalytic selectivity.

2. Experimental section

2.1. Materials

4-Bromophenylboronic acid, 2-(tributylstannyl)thiophene [2-TBS-Th], isopropanol (IPA) *N*-bromosuccinimide (NBS), acetic acid (AcOH), benzoquinone (BQ), chlorobenzene, nitromethane, iron(III) chloride [$FeCl_3$], bis(triphenylphosphine)palladium(II) dichloride[$Pd(PPh_3)_2Cl_2$], sulfuric acid (H_2SO_4), 1,2,4,5-tetrabromobenzene [BZ-4Br], bromine solution (Br_2), dibenzo-[b,d]thiophene sulfone (DBZS, 97%), benzene-1,4-diboronic acid (BZ-2BO), 95%), nitrobenzene (99%), pyrene (Py, 98%), potassium carbonate (K_2CO_3, 99.8%), triphenylphosphine (PPh_3), tetrakis(triphenylphosphine)palladium [$Pd(PPh_3)_4$, 98%], anhydrous magnesium sulfate ($MgSO_4$, 99.5%) were sourced from Sigma-Aldrich and Alfa Aesar. Details of the synthesis of 1,3,6,8-tetrakis(4-bromophenyl)pyrene (PyPh-4Br) and 3,7-dibromodibenzo[*b*,*d*]thiophene 5,5-dioxide [DBZS-2Br] can be found in the ESI† [Schemes S1 and S2, Fig. S1–S2].[39]

2.2. Synthesis of 2,5,9,12-tetrabromoanthra[1,2-*b*:4,3-*b*′:5,6-*b*″:8,7-*b*‴]tetrathiophene [ANTh-4Br]

A mixture of $Pd(PPh_3)_2Cl_2$ (192 mg, 1.08 mmol), PPh_3 (570 mg, 2.172 mmol), BZ-4Br (6 g, 15.18 mmol), and 2-TBS-Th (24.6 mL,

77.4 mmol) in 20 mL of DMF was stirred and heated at 130 °C for 16 h. After 16 h, the mixture was subjected to filtration, and the resulting solid was washed thoroughly with hexane. Recrystallization of the crude product from ethyl acetate yielded transparent white needles of 1,2,4,5-tetra(thiophen-2-yl)-benzene (BZTh, 6.1). FTIR (cm^{-1}, Fig. S3, ESI†): 3099, 1533, 1480, 1234, 847, 690. ^{1}H NMR (δ, chloroform-*d*, Fig. S4, ESI†): 6.88 (2H, s), 6.86 (4H, dd), 6.57 (8H, m). ^{13}C NMR (δ, chloroform-*d*, Fig. S5, ESI†): 141.62, 133.41, 133.24, 127.44, 127.01, 126.33. NBS (10.75 g, 62.23 mmol) and BZTh (4 g, 9.83 mmol) in THF (200 mL) at room temperature, and the reaction mixture was stirred for 16 h. The resulting white solid [1,2,4,5-tetrakis(5-bromothiophen-2-yl)benzene (BZTh-4Br)] was washed sequentially with acetone and water, and dried in an oven [5.9 g, yield: 71%]. FTIR (cm^{-1}, Fig. S6, ESI†): 3099, 1533, 1480, 1234, 847, 690. ^{1}H NMR (δ, chloroform-*d*, Fig. S7, ESI†): 7.67 (2H), 7.32 (4H), 6.95 (8H, m).

^{13}C NMR (δ, chloroform-*d*, Fig. S8, ESI†): 141.55, 133.43, 133.26, 127.36, 127.04, 126.29. A solution of $FeCl_3$ (2.43 g, 14.97 mmol) in nitromethane (41 mL) was added to BZTh-4Br (1.75 g, 2.43 mmol) in chlorobenzene (82 mL) with stirring for 60 min at room temperature. The resulting yellow precipitate was washed with DCM, 10% HCl aqueous solution for 15 min, and recrystallized from hot MeOH (400 mL) to afford ANTh-4Br (1.73 g). FTIR (cm^{-1}, Fig. S9, ESI†): 3095, 1549, 1480, 977, 789. Due to the poor solubility of ANTh-4Br in common organic solvents, the acquisition of ^{1}H and ^{13}C NMR spectra was not feasible.

2.3. Preparation of PyPh-DBZS and ANTh-DBZS CMP

A mixture of BZ-2BO (3 mmol), $Pd(PPh_3)_4$ (30 mg), PyPh-4Br (1 mmol), DBZS-2Br (1 mmol), and 2 M K_2CO_3 (10 mL) in DMF (35 mL) was added to a 100 mL Schlenk tube and the reaction was heated at 110 °C for 3 days under reflux. The crude solid was purified by Soxhlet extraction with DMF, THF, and MeOH, yielding PyPh-DBZS CMP [a green solid (yield: 78%]. For Preparation of ANTh-DBZS CMP: a mixture of BZ-2BO (3 mmol), $Pd(PPh_3)_4$ (30 mg), ANTh-4Br (1 mmol), DBZS-2Br (1 mmol), and 2 M K_2CO_3 (10 mL) in DMF (35 mL) to afford ANTh-DBZS CMP [a yellow solid (yield: 76%].

3. Results and discussion

3.1. Construction and structural elucidation of PyPh-DBZS and ANTh-DBZS CMPs photocatalysts

ANTh molecules, a polycyclic aromatic hydrocarbon enriched with sulfur atoms, possesses a highly rigid and planar π-conjugated backbone that facilitates pronounced π–π stacking and promotes effective hole transport.[40,41] These structural attributes have established ANTh as a key scaffold in the development of high-performance organic field-effect transistors (OFETs).[40,41] While functionalized ANTh derivatives have been extensively investigated in the field of organic electronics, their potential utility in photocatalytic applications, particularly in driving H_2 and H_2O_2 production, remains significantly underexplored, despite their favorable photophysical and electronic characteristics. The detailed chemical structures of the as-synthesized DBZS-2Br, and ANTh-4Br were fully characterized and confirmed by Fourier transform infrared (FTIR) spectroscopy and nuclear magnetic resonance (NMR) spectroscopy, as shown in Fig. S1–S9 (ESI†).[39–41]

In this study, a series of conjugated microporous polymers (CMPs) incorporating pyrene (PyPh), tetrathienoanthracene (ANTh), and benzothiophene *S*,*S*-dioxide (DBZS) building blocks were rationally designed and synthesized for efficient photocatalytic H_2 and H_2O_2 production. As illustrated in Fig. 1(a) and (b), the PyPh-DBZS and ANTh-DBZS CMPs were constructed *via* a Pd-catalyzed Suzuki cross-coupling polymerization. Specifically, the CMP networks were formed by coupling PyPh-4Br or ANTh-4Br with DBZS-4Br and BZ-2BO as the linker. The resulting polymerization afforded green-colored solids, corresponding to PyPh-DBZS and ANTh-DBZS CMPs, respectively. Both PyPh-DBZS and ANTh-DBZS CMPs exhibited negligible solubility and ultrastability in various organic solvents [H_2O, DMF, NMP, DMSO, and THF], consistent with their extended conjugated and highly crosslinked polymeric structures. The FTIR spectra [Fig. 2(a)] of PyPh-DBZS and ANTh-DBZS CMPs displayed peaks in 3029 and 3085 cm^{-1} for aromatic C–H, and both materials exhibited the absorption bands at 1621 and 1158 cm^{-1}, which were assigned to C=C and SO_2 units, respectively.[42–44] Solid-state ^{13}C CP/MAS NMR spectra [Fig. 2(b)] further corroborated the successful formation of extended π-conjugated frameworks in PyPh-DBZS and ANTh-DBZS CMPs. Distinct resonance signals assigned to aromatic C=C carbons appeared within the range of 139.94–129.14 ppm for PyPh-DBZS CMP, while ANTh-DBZS CMP exhibited characteristic signals spanning 140.22–124.98 ppm, confirming the incorporation of highly conjugated aromatic moieties. Thermogravimetric analysis (TGA) revealed that both PyPh-DBZS and ANTh-DBZS CMPs exhibited excellent thermal stability, retaining their structural integrity up to 590 °C.

The corresponding char yields were 74 wt% and 78 wt% for PyPh-DBZS and ANTh-DBZS CMPs, respectively [Fig. 2(c)]. The elemental compositions and chemical states of the PyPh-DBZS and ANTh-DBZS CMPs were systematically analyzed by X-ray photoelectron spectroscopy (XPS). As shown in the survey spectra [Fig. S10, ESI†], distinct signals corresponding to S 2p (~164 eV), C 1s (~284 eV), and O 1s (~531 eV) were observed for both materials, confirming their successful construction. The quantitative XPS analysis further revealed that the atomic compositions of C, O, and S in PyPh-DBZS CMP were 86.2, 2.6, and 11.1%, respectively, whereas ANTh-DBZS CMP exhibited corresponding values of 68.8, 14.9, and 16.2%, respectively, as summarized in Table S1 (ESI†). High-resolution C 1s spectra for PyPh-DBZS and ANTh-DBZS CMPs [Fig. S11 and Table S2, ESI†] revealed deconvoluted peaks at 283.7 eV and 284.5 eV, which are associated with C–C/C=C bonds and C–S linkages, respectively.

Additionally, the S 2p binding energy region [Fig. S11, ESI†] exhibited characteristic doublet peaks at 164.4 eV (S $2p_{3/2}$) and 164.9 eV (S $2p_{1/2}$), indicative of the sulfur species originating from the DBZS moieties. Nitrogen adsorption–desorption measurements at 77 K derived the Brunauer–Emmett–Teller (BET)

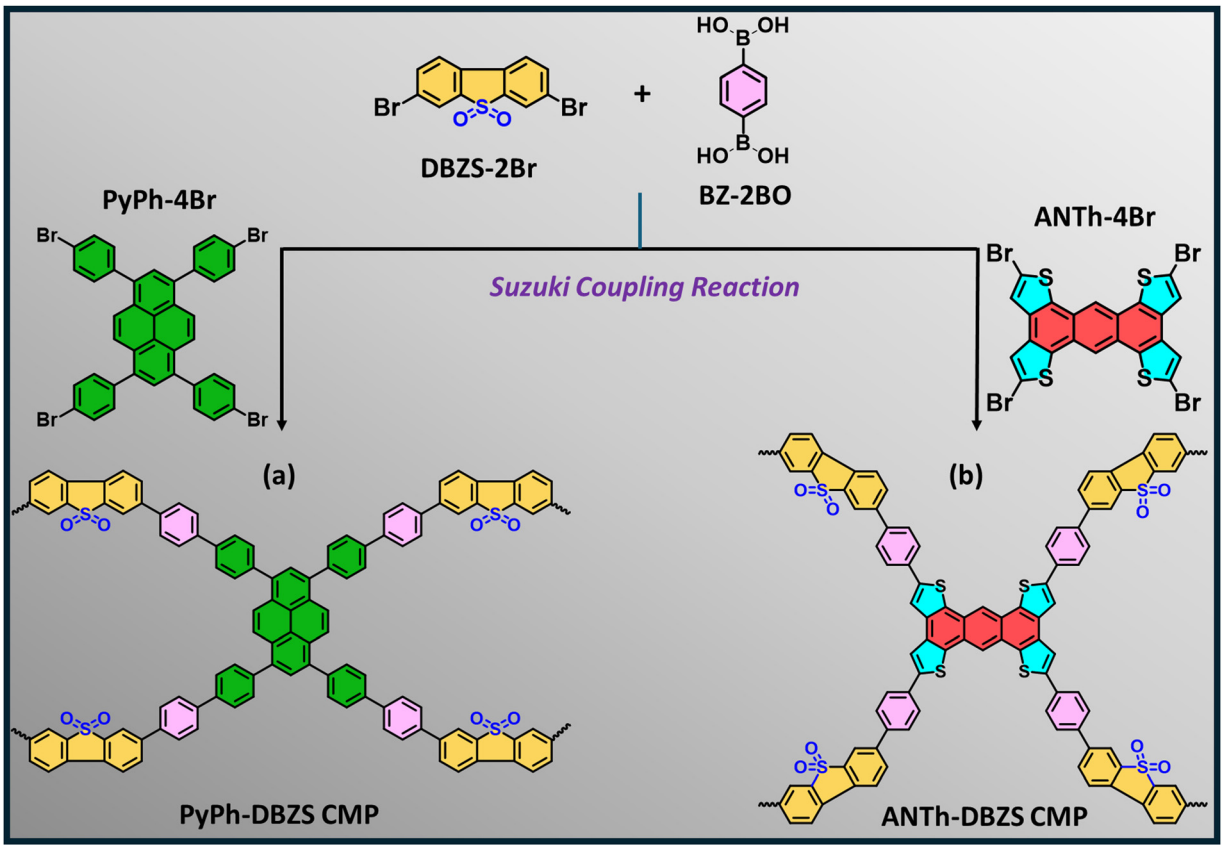

Fig. 1 Proposed synthetic strategy for (a) PyPh-DBZS and (b) ANTh-DBZS CMPs-based photocatalysts.

surface areas of PyPh-DBZS and ANTh-DBZS CMPs as 146 and 45 $m^2\ g^{-1}$, respectively [Fig. 2(d)], and the total pore volumes (P/P_0 = 0.99) as 0.185 and 0.232 $cm^3\ g^{-1}$, respectively. The BET isotherms for PyPh-DBZS and ANTh-DBZS CMPs correspond to Type II and Type III, respectively. The pore size diameters were determined using non-local density functional theory (NLDFT), and the values were 1.63 and 1.93 nm for PyPh-DBZS and ANTh-DBZS CMPs, respectively [Inset of Fig. 2(d)], indicating that these CMPs are microporous materials. The morphological features and elemental distributions of the PyPh-DBZS and ANTh-DBZS CMPs were assessed by scanning electron microscopy (SEM) coupled with energy-dispersive X-ray spectroscopy (EDS) mapping [Fig. 3]. The SEM images revealed that both CMPs exhibited irregularly shaped, aggregated particle morphologies, characteristic of conjugated polymeric networks [Fig. 3(a–f)]. Furthermore, SEM-EDS elemental mapping confirmed the homogeneous distribution of key elements, including carbon (C, red), Oxygen (O, green) and sulfur (S, yellow), throughout the polymer matrices of both PyPh-DBZS and ANTh-DBZS CMPs [Fig. 3(g–l)], validating the successful incorporation of the designed building blocks into the framework structures.

3.2. Photocatalytic hydrogen (H_2) and hydrogen peroxide (H_2O_2) production of PyPh-DBZS CMP and ANTh-DBZS CMP

In this study, we report the synthesis and photocatalytic H_2 evolution performance of two CMPs, PyPh-DBZS CMP and ANTh-DBZS CMP, constructed *via* a donor–acceptor design strategy. The CMPs feature pyrene (PyPh) and ANTh moieties as electron-donating units and DBZS as an electron-accepting unit. This molecular architecture was designed to promote effective charge carrier separation and transport, thus improving photocatalytic performance under visible-light illumination. To gain insight into the photophysical properties of the synthesized CMPs, UV-vis absorption spectroscopy was performed in *N*-methylpyrrolidone (NMP). As shown in Fig. 4(a), the ANTh-DBZS CMP exhibited a markedly red-shifted absorption onset compared to the PyPh-DBZS CMP, extending its absorption further into the visible region. This red shift is attributed to the extended π-conjugation of the anthracene core and the electron-rich fused thiophene units, which enhanced intramolecular charge delocalization.[45] The light wavelength onset of PyPh-DBZS CMP and ANTh-DBZS CMP were observed at 488 nm and 636 nm, respectively, confirming their capability to harvest visible light—a prerequisite for efficient solar-to-hydrogen conversion. The optical band gaps (E_g), estimated from Tauc plots [Fig. 4(b)], were determined to be 2.54 eV for PyPh-DBZS CMP and 1.94 eV for ANTh-DBZS CMP, placing both materials within the desirable range for visible-light-driven photocatalytic water splitting.[46–52] The results point to the feasibility of the donor–acceptor architecture in tuning light absorption and bandgap energetics for enhanced photocatalytic H_2 evolution. Beyond light-harvesting capability, the electronic

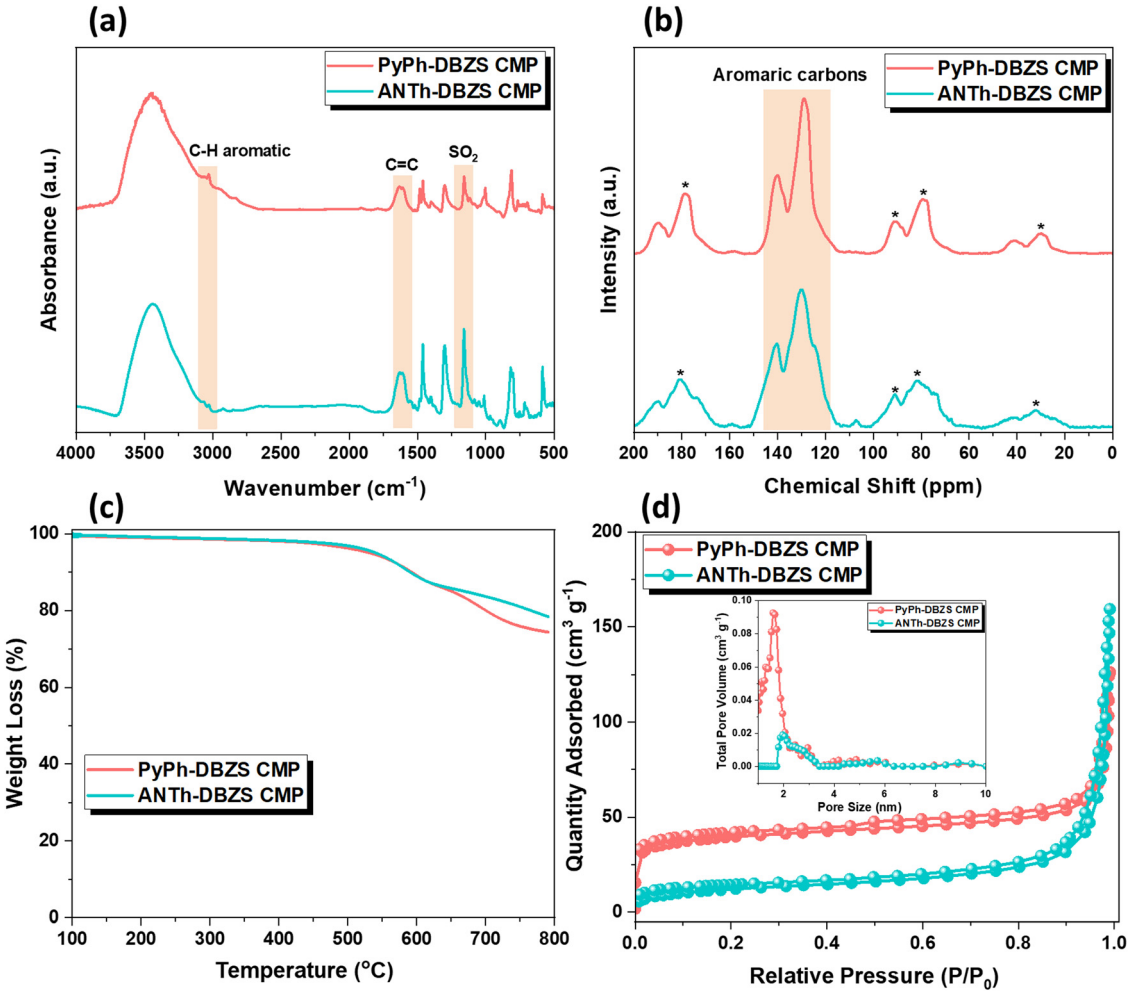

Fig. 2 (a) FTIR) spectra, (b) solid-state ^{13}CP/MAS NMR spectra, (c) TGA profiles, and (d) nitrogen adsorption–desorption isotherms of PyPh-DBZS and ANTh-DBZS CMPs [inset: associated pore size distribution plots].

structure of the CMPs plays a pivotal role in governing their photocatalytic performance. To evaluate the frontier orbital energy levels, cyclic voltammetry (CV) measurements were conducted. As shown in Fig. S12 (ESI†) and summarized in Table 1, the highest occupied molecular orbital (HOMO) energy levels of PyPh-DBZS CMP and ANTh-DBZS CMP were calculated to be −5.23 eV and −5.05 eV, respectively, reflecting their electron-donating characteristics. The corresponding lowest unoccupied molecular orbital (LUMO) energy levels, approximated from the optical band gaps and HOMO positions, were calculated to be −2.68 eV for PyPh-DBZS CMP and −3.11 eV for ANTh-DBZS CMP [Fig. 4c]. Notably, both CMPs exhibit LUMO energy levels that are thermodynamically favorable for proton reduction, confirming their suitability for photocatalytic H_2 evolution.[53,54] Guided by the photophysical and electronic properties of the CMPs, we next evaluated their photocatalytic H_2 evolution.

Photocatalytic experiments were executed at 25 °C in a 40 mL sealed photoreactor. To improve the dispersion of the DBZS-based CMPs in aqueous media, NMP was employed as a co-solvent. Ascorbic acid (AA) served as a sacrificial electron donor to effectively scavenge photogenerated holes, while an *in situ* photo-deposited platinum (Pt) co-catalyst, introduced *via* H_2PtCl_6, was used to facilitate charge separation and accelerate hydrogen evolution. The influence of Pt co-catalyst loading on photocatalytic efficiency was explored by varying the amount of H_2PtCl_6 from 2 to 6 wt% under $\lambda > 420$ nm for 4 h in the presence of 0.1 M AA as a sacrificial agent. The HER was monitored throughout the irradiation period to assess the catalytic performance, as shown in Fig. 5(a) and (b). The HER was strongly dependent on the concentration of the sacrificial electron donor, with the highest activity observed at an AA concentration of 0.1 M. Notably, a Pt loading of 2 wt% afforded the optimal HER, beyond which a decrease in activity was observed, likely due to excessive Pt coverage hindering light absorption and active site accessibility. We further investigated the influence of photocatalyst loading by varying the mass of PyPh-DBZS CMP from 1.0 to 5.0 mg [Fig. 5(c)]. Interestingly, an inverse correlation between photocatalyst loading and HER was observed, with the highest activity achieved at a loading of 1.0 mg. This trend is attributed to the attenuation of light penetration and reduced photocatalyst utilization at higher concentrations, consistent with previous activity [Fig. 5(d)].[55]

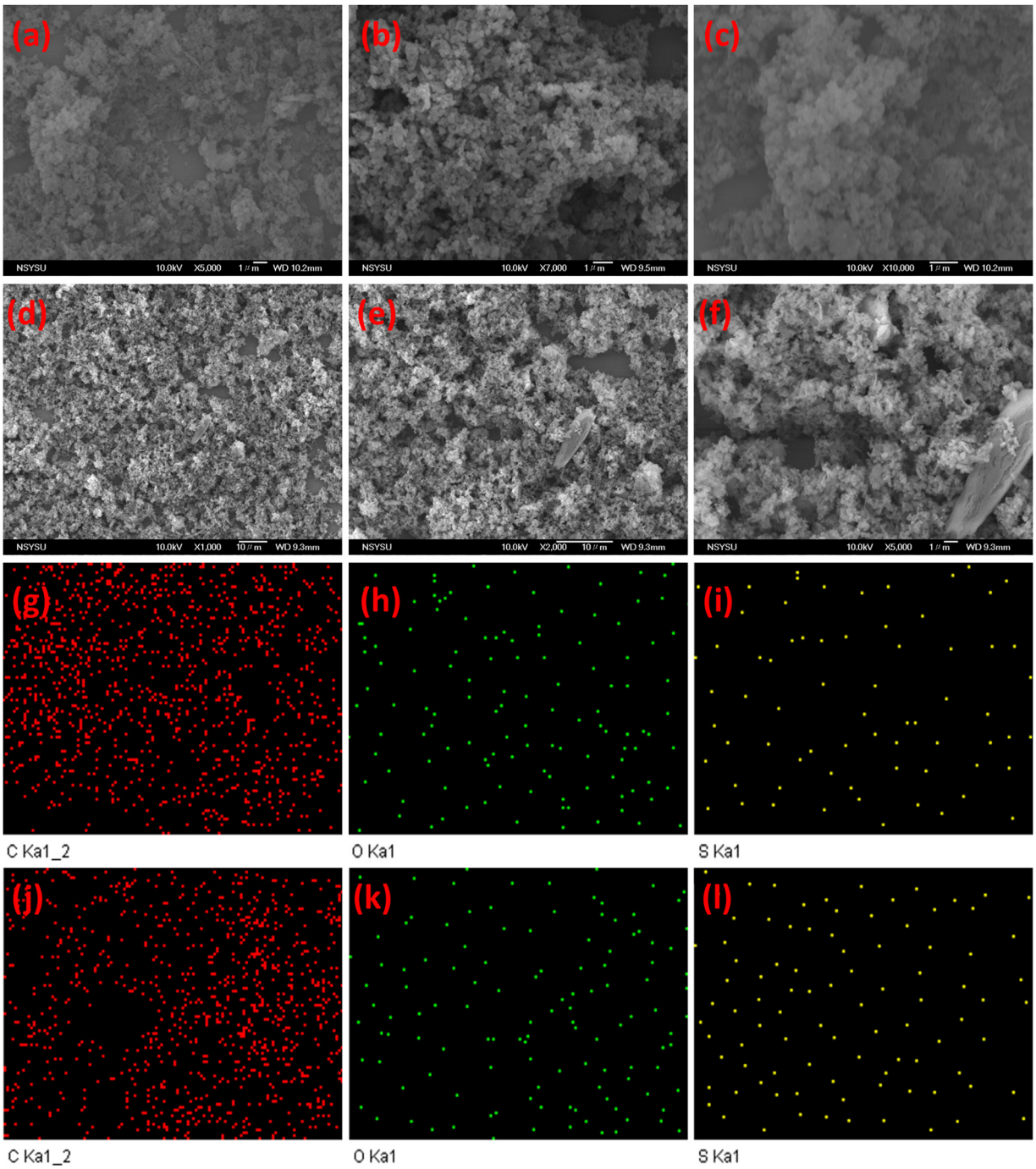

Fig. 3 (a)–(f) SEM and (g)–(l) SEM-EDS mapping images for (a)–(c) and (g)–(i) PyPh-DBZS and (d)–(f) and (j)–(l) ANTh-DBZS CMPs photocatalysts.

Under optimized conditions, PyPh-DBZS CMP exhibited an outstanding HER of 133 241 μmol g^{-1} h^{-1}, highlighting the effectiveness of the donor–acceptor design combining the strong electron-donating pyrene unit with the electron-deficient DBZS moiety. In contrast, ANTh-DBZS CMP demonstrated a lower HER of 34 791 μmol g^{-1} h^{-1}, underscoring the critical role of the molecular structure in governing photocatalytic the reproducibility of our results, the HER of PyPh-DBZS CMP was evaluated across three independently synthesized batches, with error bars confirming the consistency of the performance [Fig. 5(e)]. Notably, the HER of the PyPh-DBZS and ANTh-DBZS CMPs photocatalysts was also compared with those of other reported polymeric photocatalysts, including g-C_3N_4, CMPs, covalent organic polymers (COPs), and covalent organic frameworks (COFs) [Table S3, ESI†]. The activities of the PyPh-DBZS and ANTh-DBZS CMPs photocatalysts (5 mg) in the absence of the Pt cocatalyst were 25 103 μmol g^{-1} h^{-1} for PyPh-DBZS CMP and 8101 μmol g^{-1} h^{-1} for ANTh-DBZS CMP,

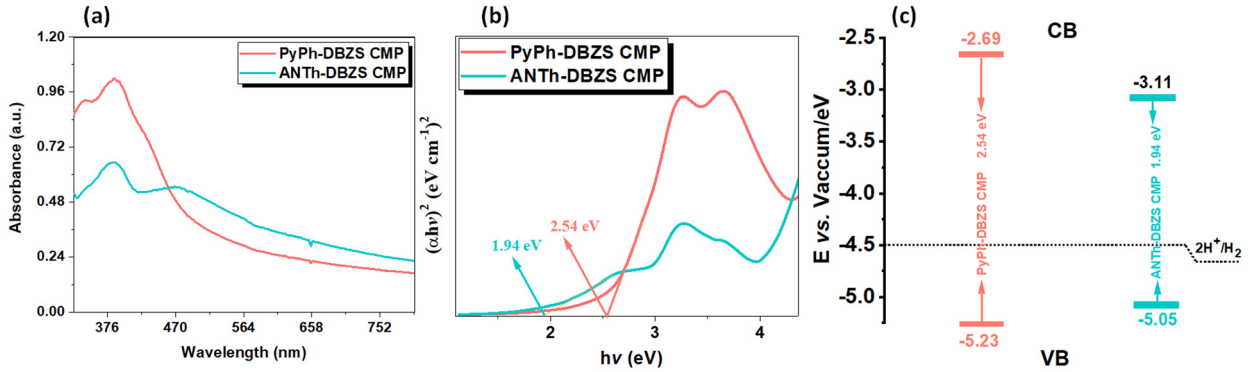

Fig. 4 (a) UV-vis absorption spectra, (b) corresponding Tauc plots for optical band gap estimation, and (c) schematic energy level diagrams of PyPh-DBZS and ANTh-DBZS CMPs photocatalysts.

Table 1 Photophysical properties and HER of the PyPh-DBZS and ANTh-DBZS CMPs photocatalysts

CMPs	HOMO/LUMO (eV)	Bandgap (eV)	Wavelength onset (nm)	HER (μmol g^{-1} h^{-1})	AQY (%)	
					420 nm	460 nm
PyPh-DBZS CMP	−5.23/−2.69	2.54	488	133 214	21.6	9.70
ANTh-DBZS CMP	−5.05/−3.11	1.94	636	34 791	5.6	4.8

which are both about three times lower than their activities in the presence of Pt [Fig. S13, ESI†]. To further evaluate the photocatalytic efficiency of the PyPh-DBZS and ANTh-DBZS CMPs, the apparent quantum yield (AQY) for H_2 evolution was determined using monochromatic light at 420 nm and 460 nm, controlled by bandpass filters [Fig. 5(f)]. The AQY reflects the fraction of incident photons effectively converted into hydrogen molecules. Notably, PyPh-DBZS CMP exhibited a remarkable AQY of 21.6% at 420 nm, underscoring its excellent photon-to-hydrogen conversion efficiency and further confirming its potential as a potent photocatalyst activated under visible-light irradiation. Besides, it is necessary to provide some experiments to prove that the photocatalytic activities of H_2 and H_2O_2 evolution over the present catalysts originate from the photocatalytic process rather than other pathways such as the self-decomposition of catalysts. The two CMP materials were analyzed by FTIR before and after the photocatalytic experiments. From the obtained spectra, we confirmed that the materials are stable during the reaction, as the FTIR spectra showed no notable differences before and after the reaction, as illustrated in Fig. S14 (ESI†). The photocatalytic activities of ANTh-DBZS and PyPh-DBZS CMPs were further assessed toward photocatalytic generation of hydrogen H_2O_2 in the presence of ethanol as a sacrificial agent, which served as an effective hole scavenger. The concentration of H_2O_2 was quantitatively determined *via* the Ce^{4+} colorimetric method. The corresponding evolution of the absorption intensity and calibration curve is presented in Fig. S15(a) and (b) (ESI†), respectively. As shown in Fig. 6(a), the ANTh-DBZS CMP achieved a significantly higher H_2O_2 evolution rate of 24.51 mM g^{-1} over 3 h, outperforming the PyPh-DBZS CMP, which exhibited a production rate of 4.76 mM g^{-1} under identical conditions. These results highlight that the molecular integration of ANTh and DBZS units within the polymeric framework is more advantageous for promoting photocatalytic H_2O_2 generation than the coupling of Py and DBZS moieties. To elucidate the influence of distinct scavenging agents on photocatalytic H_2O_2 production by ANTh-DBZS CMP, a series of control experiments were conducted under identical reaction conditions. In addition to the scavenger-free system, specific quenchers were employed to capture reactive oxygen species (ROS) generated during the photocatalytic process. IPA and BQ were introduced as selective scavengers for hydroxyl radicals ($^{\bullet}OH$) and superoxide radicals ($O_2^{\bullet-}$), respectively. In Fig. 6(b), it is shown that H_2O_2 evolution rates of scavenger-free and ethanol (hole scavenger)-containing samples are similar. This means that the concerted two-hole-mediated oxidation of water is ruled out as a potential pathway (see SI explanatory text). Furthermore, it is noted that the potential of the aforementioned half-reaction (−6.26 eV) is not in a thermodynamically favored position when compared with the valence band of both photocatalysts [Fig. 4(c)]. Similarly, the potential of water oxidation to hydroxy radicals (one-electron process) stands in more negative value (−7.23 eV) than the HOMO of any of the photocatalysts. This makes the oxidative formation of hydroxy radical a non-feasible thermodynamic process. By using isopropanol as a typical hydroxy radical scavenger, only a slight inhibition of H_2O_2 evolution was observed. This means that H_2O_2 evolution is not favored through water oxidation pathways. Regarding the reductive pathways through the conduction band, a partial suppression of peroxide formation was observed in the presence of benzoquinone (a superoxide radical scavenger). This implies that H_2O_2 formation may take place through a stepwise oxygen reduction to some extent. We strongly suggest that the dominant pathway for H_2O_2 formation is

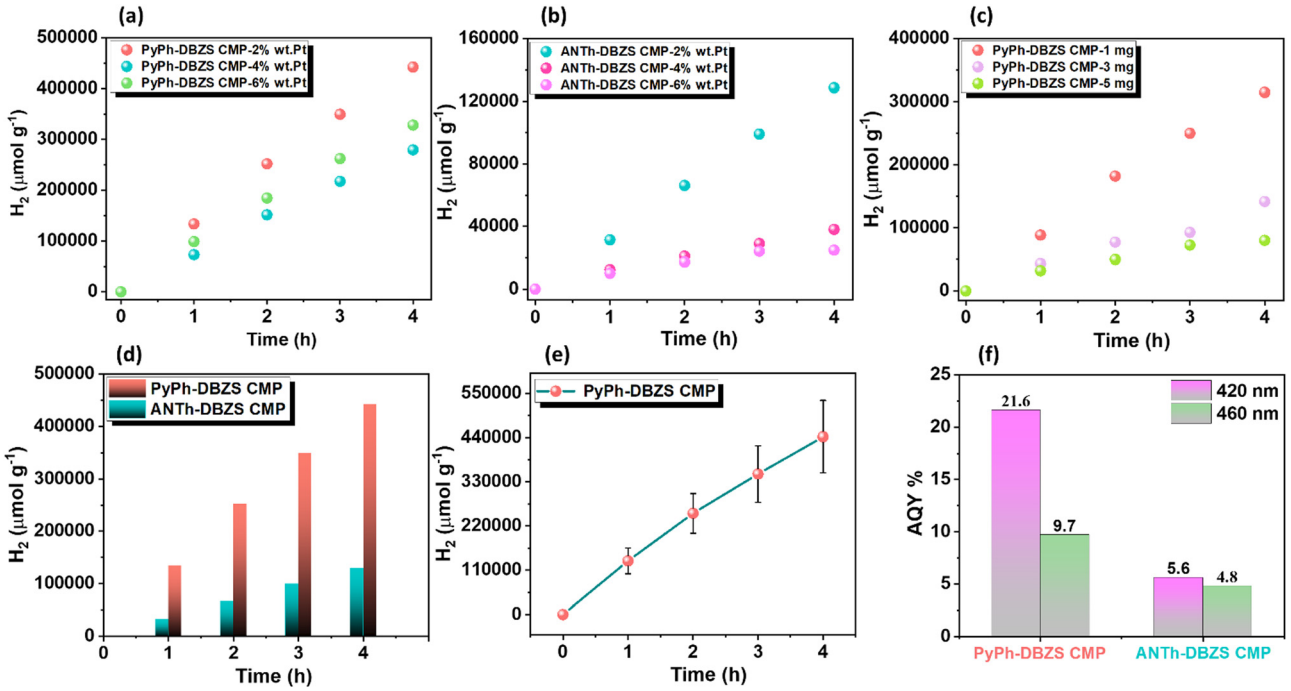

Fig. 5 (a) and (b) Effect of different weight % of Pt on HER of PyPh-DBZS and ANTh-DBZS CMPs, respectively [AA concentration of 0.1 M]; (c) effect of different weight loading of PyPh-DBZS CMP, (d) time dependent HER of PyPh-DBZS and ANTh-DBZS CMPs [1 mg and 2% wt Pt], (e) time dependent HER of three batches with error bar for PyPh-DBZS CMP, (f) AQYs of the PyPh-DBZS and ANTh-DBZS CMPs at various wavelengths of light.

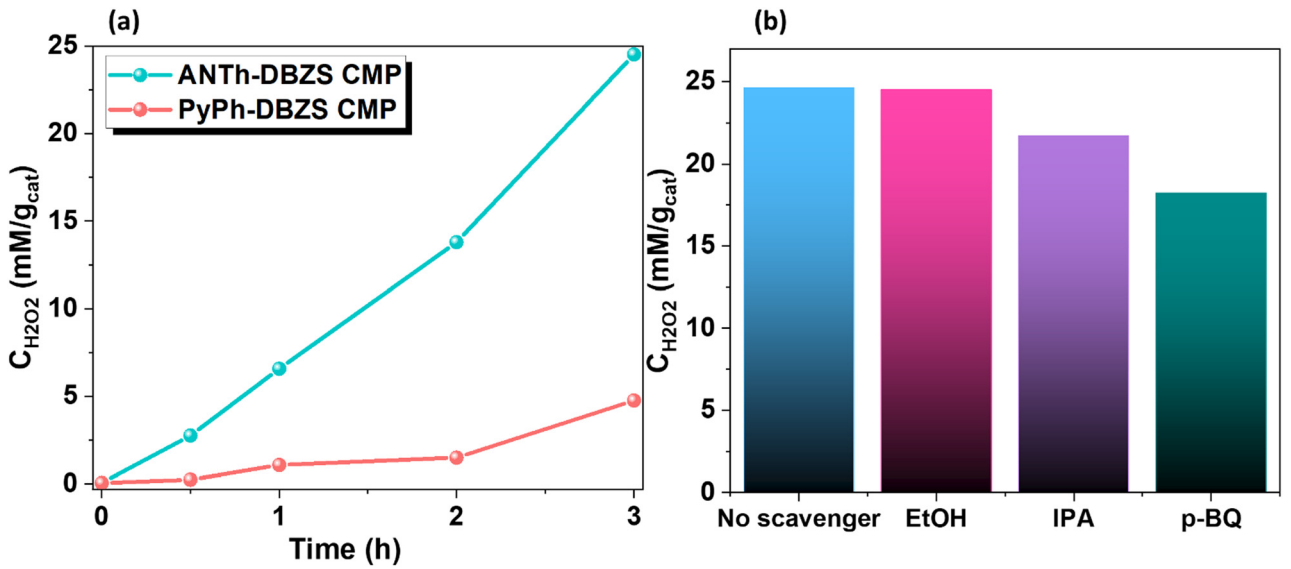

Fig. 6 (a) Time-dependent H_2O_2 photogeneration under visible light irradiation for ANTh-DBZS and PyPh-DBZ CMPs and (b) experiments of H_2O_2 generation under different scavengers for ANTh-DBZS CMP.

the concerted oxygen reduction, followed by the stepwise reductive process as a secondary path.

4. Conclusions

In summary, we have successfully developed D–A photoactive porous organic photocatalysts, namely PyPh-DBZS CMP and ANTh-DBZS CMP, through a facile and robust Suzuki coupling polymerization strategy. These materials integrate electron-donating units (PyPh and ANTh) with an electron-accepting DBZS moiety, affording CMPs with desirable structural and functional attributes. Both CMPs exhibit outstanding thermal stability ($T_{d_{10}}$ up to 590 °C), moderate Brunauer–Emmett–Teller (BET) surface areas, and a microporous architecture conducive to enhanced charge transport and separation. Photocatalytic

evaluations reveal that PyPh-DBZS CMP achieves an impressive HER of 133 241 μmol g^{-1} h^{-1} under visible-light irradiation, highlighting its superior photocatalytic performance. Notably, ANTh-DBZS CMP exhibits structure-dependent photophysical behavior, promoting efficient charge separation and delivering enhanced photocatalytic selectivity for H_2O_2 production, achieving a yield of 24.51 mM g^{-1}. These findings provide valuable insights into the rational design of next-generation D–A CMP photocatalysts for sustainable hydrogen production and H_2O_2 generation under visible-light-driven conditions.

Author contributions

Mohamed Gamal Mohamed: conceptualization, formal analysis, writing – original draft, investigation, methodology, validation, writing – review & editing, Supervision. Islam M. A. Mekhemer: investigation, visualization, methodology, writing – review & editing. Ahmed F. H. Selim: conceptualization, formal analysis, writing – original draft. Andreas Katsamitros: formal analysis, investigation. Dimitrios Tasis: writing – original draft, resources, supervision. Abdul Basit: formal analysis. Ho-Hsiu Chou: resources, supervision. Shiao-Wei Kuo: resources, supervision.

Data availability

The data that support the findings of this study are available.

Conflicts of interest

There are no conflicts to declare.

Acknowledgements

This study was supported financially by the National Science and Technology Council, Taiwan, under contracts NSTC 113-2223-E-110-001- and 113-2221-E-110-012-MY3. The authors thank the staff at National Sun Yat-sen University for their assistance with the TEM (ID: EM022600) experiments.

Notes and references

1 F. F. Wang, O. Li and D. S. Xu, Recent Progress in Semiconductor-Based Nanocomposite Photocatalysts for Solar-to-Chemical Energy Conversion, *Adv. Energy Mater.*, 2017, **7**, 1700529, DOI: **10.1002/aenm.201700529**.

2 D. Franchi and Z. Amara, Applications of Sensitized Semiconductors as Heterogeneous Visible-Light Photocatalysts in Organic Synthesis, *ACS Sustainable Chem. Eng.*, 2020, **8**, 15405–15429, DOI: **10.1021/acssuschemeng.0c05179**.

3 K. Ullah, M. Amin, P. Zhao, N. Qin and A. W. Xu, Recent advances in inorganic oxide semiconductor-based S-scheme heterojunctions for photocatalytic hydrogen evolution, *Inorg. Chem. Front.*, 2025, **12**, 1329–1348, DOI: **10.1039/D4QI02797C**.

4 A. Kubacka, M. F. Garcia and G. Colon, Advanced nanoarchitectures for solar photocatalytic applications, *Chem. Rev.*, 2012, **112**, 15555, DOI: **10.1021/cr100454n**.

5 J. Low, J. Yu, M. Jaroniec, S. Wageh and A. A. Al-Ghamdi, Heterojunction Photocatalysts, *Adv. Mater.*, 2017, **29**, 1601694, DOI: **10.1002/adma.201601694**.

6 M. Q. Yang, N. Zhang, M. Pagliaro and Y.-J. Xu, Artificial photosynthesis over graphene–semiconductor composites. Are we getting better?, *Chem. Soc. Rev.*, 2014, **43**, 8240–8254, DOI: **10.1039/C4CS00213J**.

7 B. J. Smith, A. C. Overholts, N. Hwang and W. R. Dichtel, Insight into the crystallization of amorphous imine-linked polymer networks to 2D covalent organic frameworks, *Chem. Commun.*, 2016, **52**, 3690–3693, DOI: **10.1039/C5CC10221A**.

8 M. G. Mohamed, C. C. Chen, M. Ibrahim, A. O. Mousa, M. H. Elsayed, Y. Ye and S. W. Kuo, Tetraphenylanthraquinone and Dihydroxybenzene-Tethered Conjugated Microporous Polymer for Enhanced CO_2 Uptake and Supercapacitive Energy Storage, *JACS Au*, 2024, **4**, 3593–3605, DOI: **10.1021/jacsau.4c0053.7**.

9 W. T. Chung, I. M. A. Mekhemer, M. G. Mohamed, A. M. Elewa, A. F. M. EL-Mahdy, H. H. Chou, S. W. Kuo and K. C. W. Wu, Recent advances in metal/covalent organic frameworks based materials: Their synthesis, structure design and potential applications for hydrogen production, *Coord. Chem. Rev.*, 2023, **483**, 215066, DOI: **10.1016/j.ccr.2023.215066**.

10 M. M. Samy, M. G. Mohamed, S. U. Sharma, S. V. Chaganti, J. T. Lee and S. W. Kuo, An Ultrastable Tetrabenzonaphthalene-Linked conjugated microporous polymer functioning as a high-performance electrode for supercapacitors, *J. Taiwan Inst. Chem. Eng.*, 2024, **158**, 104750, DOI: **10.1016/j.jtice.2023.104750**.

11 A. Basit, Y. C. Kao, Y. A. El-Ossaily, S. W. Kuo and M. G. Mohamed, Rational engineering and synthesis of pyrene and thiazolo[5,4-d] thiazole-functionalized conjugated microporous polymers for efficient supercapacitor energy storage, *J. Mater. Chem. A*, 2024, **12**, 30508–30521, DOI: **10.1039/D4TA05908E**.

12 M. G. Mohamed, W. C. Chang and S. W. Kuo, Crown ether- and benzoxazine-linked porous organic polymers displaying enhanced metal ion and CO_2 capture through solid-state chemical transformation, *Macromolecules*, 2022, **55**, 7879–7892, DOI: **10.1021/acs.macromol.2c01216**.

13 M. G. Mohamed, A. F. M. EL-Mahdy, M. G. Kotp and S. W. Kuo, Advances in porous organic polymers: syntheses, structures, and diverse applications, *Mater. Adv.*, 2022, **3**, 707–733, DOI: **10.1039/D1MA00771H**.

14 M. M. Samy, I. M. A. Mekhemer, M. G. Mohamed, M. H. Elsayed, K. H. Lin, Y. K. Chen, T. L. Wu, H. H. Chou and S. W. Kuo, Conjugated microporous polymers incorporating Thiazolo [5, 4-d] thiazole moieties for Sunlight-Driven hydrogen production from water, *Chem. Eng. J.*, 2022, **446**, 137158, DOI: **10.1016/j.cej.2022.137158**.

15 S. Y. Chang, A. M. Elewa, M. G. Mohamed, I. M. A. Mekhemer, M. M. Samy, K. Zhang, H. H. Chou and

S. W. Kuo, Rational design and synthesis of bifunctional Dibenzo [g, p] chrysene-based conjugated microporous polymers for energy storage and visible light-driven photocatalytic hydrogen evolution, *Mater. Today Chem.*, 2023, **33**, 101680, DOI: **10.1016/j.mtchem.2023.101680**.

16 M. G. Mohamed, S. U. Sharma, P. T. Wang, M. Ibrahim, M. H. Lin, C. L. Liu, M. Ejaz, H. J. Yen and S. W. Kuo, Construction of fully π-conjugated, diyne-linked conjugated microporous polymers based on tetraphenylethene and dibenzo [g, p] chrysene units for energy storage, *Polym. Chem.*, 2024, **15**, 2827–2839, DOI: **10.1039/D4PY00421C**.

17 J.-X. Jiang, F. Su, A. Trewin, C. D. Wood, N. L. Campbell, H. Niu, C. Dickinson, A. Y. Ganin, M. J. Rosseinsky, Y. Z. Khimyak and A. I. Cooper, Conjugated microporous poly(aryleneethynylene) networks, *Angew. Chem., Int. Ed.*, 2007, **46**, 8574–8578, DOI: **10.1002/anie.200701595**.

18 J. Lee and A. I. Cooper, Advances in Conjugated Microporous Polymers, *Chem. Rev.*, 2020, **120**, 2171–2214, DOI: **10.1021/acs.chemrev.9b00399**.

19 R. S. Sprick, B. Bonillo, M. Sachs, R. Clowes, J. R. Durrant, D. J. Adams and A. I. Cooper, Extended conjugated microporous polymers for photocatalytic hydrogen evolution from water, *Chem. Commun.*, 2016, **52**, 10008–10011, DOI: **10.1039/C6CC03536A**.

20 B. Wang, Z. Xie, Y. Li, Z. Yang and L. Chen, Dual-Functional Conjugated Nanoporous Polymers for Efficient Organic Pollutants Treatment in Water: A Synergistic Strategy of Adsorption and Photocatalysis, *Macromolecules*, 2018, **51**, 3443–3449, DOI: **10.1021/acs.macromol.8b00669**.

21 Z. Tang, S. Xu, Y. Yang, T. Wang, H. He, X. Lin, Y. Zhou and Z. Zou, Reaction Site Designation by Intramolecular Electric Field in Tröger's-Base-Derived Conjugated Microporous Polymer for Near-Unity Selectivity of CO_2 Photoconversion, *Adv. Mater.*, 2023, **35**, 2210693, DOI: **10.1002/adma.202210693**.

22 X. Xu, R. Sa, W. Huang, Y. Sui, X. Li, Y. Li and H. Zhong, Conjugated Organic Polymers with Anthraquinone Redox Centers for Efficient Photocatalytic Hydrogen Peroxide Production from Water and Oxygen under Visible Light Irradiation without Any Additives, *ACS Catal.*, 2022, **12**, 12954–12963, DOI: **10.1021/acscatal.2c04085**.

23 A. Katsamitros, A. N. Giannakakis, N. Karamoschos, N. Karousis and D. Tasis, Covalent Organic Frameworks for Photocatalytic Hydrogen Peroxide Evolution, *Chem. – Eur. J.*, 2025, **31**, e202404272, DOI: **10.1002/chem.202404272**.

24 Z. Wang, X. Yang, T. Yang, Y. Zhao, F. Wang, Y. Chen, J. H. Zeng, C. Yan, F. Huang and J.-X. Jiang, Dibenzothiophene Dioxide Based Conjugated Microporous Polymers for Visible-Light-Driven Hydrogen Production, *ACS Catal.*, 2018, **8**, 8590–8596, DOI: **10.1021/acscatal.8b02607**.

25 Y. Zhao, W. Ma, Y. Xu, C. Zhang, Q. Wang, T. Yang, X. Gao, F. Wang, C. Yan and J.-X. Jiang, Effect of Linking Pattern of Dibenzothiophene-S,S-dioxide-Containing Conjugated Microporous Polymers on the Photocatalytic Performance, *Macromolecules*, 2018, **51**, 9502–9508, DOI: **10.1021/acs.macromol.8b02023**.

26 Z.-A. Lan, W. Ren, X. Chen, Y. Zhang and X. Wang, Conjugated donor-acceptor polymer photocatalysts with electron-output "tentacles" for efficient hydrogen evolution, *Appl. Catal., B*, 2019, **245**, 596–603, DOI: **10.1016/j.apcatb.2019.01.010**.

27 X. Gao, C. Shu, C. Zhang, W. Ma, S.-B. Ren, F. Wang, Y. Chen, J. H. Zeng and J.-X. Jiang, Substituent effect of conjugated microporous polymers on the photocatalytic hydrogen evolution activity, *J. Mater. Chem. A*, 2020, **8**, 2404–2411, DOI: **10.1039/C9TA13212K**.

28 C. Shu, C. Han, X. Yang, C. Zhang, Y. Chen, S. Ren, F. Wang, F. Huang and J.-X. Jiang, Boosting the Photocatalytic Hydrogen Evolution Activity for D–π–A Conjugated Microporous Polymers by Statistical Copolymerization, *Adv. Mater.*, 2021, **33**, 2008498, DOI: **10.1002/adma.202008498**.

29 R. S. Sprick, Y. Bai, A. A. Y. Guilbert, M. Zbiri, C. M. Aitchison, L. Wilbraham, Y. Yan, D. J. Woods, M. A. Zwijnenburg and A. I. Cooper, Photocatalytic Hydrogen Evolution from Water Using Fluorene and Dibenzothiophene Sulfone-Conjugated Microporous and Linear Polymers, *Chem. Mater.*, 2019, **31**, 305–313, DOI: **10.1021/acs.chemmater.8b02833**.

30 P. Xie, C. Han, S. Xiang, S. Jin, M. Ge, C. Zhang and J.-X. Jiang, Toward high-performance dibenzo[g,p]chrysene-based conjugated polymer photocatalysts for photocatalytic hydrogen production through donor-acceptor-acceptor structure design, *Chem. Eng. J.*, 2023, **459**, 141553, DOI: **10.1016/j.cej.2023.141553**.

31 J. Wang, G. Ouyang, Y. Wang, X. Qiao, W.-S. Li and H. Li, 1,3,5-Triazine and dibenzo[b,d]thiophene sulfone based conjugated porous polymers for highly efficient photocatalytic hydrogen evolution, *Chem. Commun.*, 2020, **56**, 1601–1604, DOI: **10.1039/C9CC08412F**.

32 C. Ru, T. Zhou, J. Zhang, X. Wu, P. Sun, P. Chen, L. Zhou, H. Zhao, J. Wu and X. Pan, Introducing Secondary Acceptors into Conjugated Polymers to Improve Photocatalytic Hydrogen Evolution, *Macromolecules*, 2021, **54**, 8839–8848, DOI: **10.1021/acs.macromol.1c00705**.

33 F. Li, X. Dai, L. Zhang, H. Wu, J. Li, J. Guo and Q. Yi, Triphenylamine promoted geometric structure adjusting of the novel macrocyclic structure D-π-A conjugated microporous polymers for photocatalytic hydrogen evolution, *Fuel*, 2024, **370**, 131812, DOI: **10.1016/j.fuel.2024.131812**.

34 M. Sarkar and A. Patra, N,N′-octyl biphenothiazine and dibenzothiophene dioxide-based soluble porous organic polymer for biphasic photocatalytic hydrogen evolution, *Chem. Commun.*, 2023, **59**, 2584–2587, DOI: **10.1039/D2CC06321B**.

35 X. Liu, W. Zhang, J. Zhao, Y. Du and F. Zhao, Enhanced delocalization and separation of charge carriers of D-π-A type conjugated porous polymers by inserting fused thiophene derivative as π bridge for improved photocatalytic activity, *Fuel*, 2025, **387**, 134347, DOI: **10.1016/j.fuel.2025.134347**.

36 R. Liang, J. Luo, S. Lin, Z. Li, Z. Dong, Y. Wu, Y. Wang, X. Cao, C. Meng, F. Yu, Y. Liu and Z. Zhang, Boosting the

photoreduction uranium activity for donor–acceptor–acceptor type conjugated microporous polymers by statistical copolymerization, *Sep. Purif. Technol.*, 2023, **312**, 123291, DOI: **10.1016/j.seppur.2023.123291**.

37 H. Yan, Y. Deng, M. Shen, Y.-X. Ye, X. Yang and G. Ouyang, Regulation the reactive oxygen species on conjugated polymers for highly efficient photocatalysis, *Appl. Catal., B*, 2022, **314**, 121488, DOI: **10.1016/j.apcatb.2022.121488**.

38 X. Luo, S. Zhou, P. Wang, D. Wang and P. Gu, A near-infrared-II light-response BODIPY-based conjugated microporous polymer for enhanced photocatalytic degradation of cationic dyes and H_2O_2 production, *Chem. Commun.*, 2024, **60**, 7910–7913, DOI: **10.1039/D4CC02912G**.

39 A. Basit, M. G. Mohamed, S. U. Sharma and S. W. Kuo, Thianthrene- and Thianthrene Tetraoxide-Functionalized Conjugated Microporous Polymers for Efficient Energy Storage, *ACS Appl. Polym. Mater.*, 2024, **6**, 12247–12260, DOI: **10.1021/acsapm.4c02368**.

40 C. A. Wang, J. P. Zhang, K. Nie, Y. W. Li, Q. Li, G. Z. Jiao, J. G. Chang and Y. F. Han, Tetrathienoanthracene-functionalized Conjugated Microporous Polymers As an Efficient, Metal-Free Visible-Light Solid Organocatalyst for Heterogeneous Photocatalysis, *Catal. Sci. Technol.*, 2021, **11**, 3799–3809, DOI: **10.1039/D1CY00488C**.

41 L. Jaclyn, O. D. Brusso, A. D. Hirst, G. Srinivasan, C. Fabio, M. R. Craig, T. O. Richard, R. D. Federico and F. Dmitrii, Perepichka. Two-Dimensional Structural Motif in Thienoacene Semiconductors: Synthesis, Structure, and Properties of Tetrathienoanthracene Isomers, *Chem. Mater.*, 2008, **20**, 2482–2494, DOI: **10.1021/cm7030653**.

42 C. Shu, Y. Zhao, C. Zhang, X. Gao, W. Ma, S. B. Ren, F. Wang, Y. Chen, J. H. Zeng and J. X. Jiang, Bisulfone-Functionalized Organic Polymer Photocatalysts for High-Performance Hydrogen Evolution, *ChemSusChem*, 2020, **13**, 369–375, DOI: **10.1002/cssc.201902797**.

43 M. G. Mohamed, S. Y. Chang, M. Ejaz, M. M. Samy, A. O. Mousa and S. W. Kuo, Design and synthesis of bisulfone-linked two-dimensional conjugated microporous polymers for CO_2 adsorption and energy storage, *Molecules*, 2023, **28**, 3234, DOI: **10.3390/molecules28073234**.

44 M. G. Mohamed, H. Y. Hu, S. Santhoshkumar, M. Madhu, T. H. Mansoure, C. W. Hsiao, Y. Ye, C. W. Huang, W. L. Tseng and S. W. Kuo, Design and Synthesis of Bifunctional Conjugated Microporous Polymers Containing Tetraphenylethene and Bisulfone Units for Energy Storage and Fluorescent Sensing of p-Nitrophenol, *Colloids Surf., A*, 2024, **680**, 132675, DOI: **10.1016/j.colsurfa.2023.132675**.

45 G. Saranya, K. Navamani and K. Senthilkumar, A theoretical study on optical and charge transport properties of anthra-[1, 2-b: 4, 3-b′: 5, 6-b ″: 8, 7-b‴] tetrathiophene molecules, *Chem. Phys.*, 2014, **433**, 48–59, DOI: **10.1016/j.chemphys.2014.01.020**.

46 I. M. A. Mekhemer, A. M. Elewa, M. M. Elsenety, M. M. Samy, M. G. Mohamed, A. F. Musa, T. F. Huang, T. C. Wei, S. W. Kuo, B. H. Chen, S. D. Yang and H. H. Chou, Self-condensation for enhancing the hydrophilicity of covalent organic polymers and photocatalytic hydrogen generation with unprecedented apparent quantum yield up to 500 nm, *Chem. Eng. J.*, 2024, **497**, 154280, DOI: **10.1016/j.cej.2024.154280**.

47 M. G. Mohamed, M. H. Elsayed, C. J. Li, A. E. Hassan, I. M. A. Mekhemer, A. F. Musa, M. K. Hussien, L. C. Chen, K. H. Chen, H. H. Chou and S. W. Kuo, Reticular design and alkyne bridge engineering in donor–π–acceptor type conjugated microporous polymers for boosting photocatalytic hydrogen evolution, *J. Mater. Chem. A*, 2024, **12**, 7693–7710, DOI: **10.1039/D3TA07309B**.

48 S. U. Sharma, M. H. Elsayed, I. M. A. Mekhemer, T. S. Meng, H. H. Chou, S. W. Kuo and M. G. Mohamed, Rational design of pyrene and thienyltriazine-based conjugated microporous polymers for high-performance energy storage and visible-light photocatalytic hydrogen evolution from water, *Giant*, 2024, **17**, 100217, DOI: **10.1016/j.giant.2023.100217**.

49 M. H. Elsayed, M. Abdellah, A. Z. Alhakemy, I. M. A. Mekhemer, A. E. A. Aboubakr, B. H. Chen, A. Sabbah, K. H. Lin, W. S. Chiu, S. J. Lin, C. Y. Chu, C. H. Lu, S. D. Yang, M. G. Mohamed, S. W. Kuo, C. H. Hung, L. C. Chen, K. H. Chen and H. H. Chou, Overcoming small-bandgap charge recombination in visible and NIR-light-driven hydrogen evolution by engineering the polymer photocatalyst structure, *Nat. Commun.*, 2024, **15**, 707, DOI: **10.1038/s41467-024-45085-6**.

50 M. G. Mohammed, M. H. Elsayed, Y. Ye, M. M. Samy, A. E. Hassan, T. H. Mansoure, Z. Wen, H. H. Chou, H. K. Chen and S. W. Kuo, Construction of Porous Organic/Inorganic Hybrid Polymers Based on Polyhedral Oligomeric Silsesquioxane for Energy Storage and Hydrogen Production from Water, *Polymers*, 2023, **15**, 182, DOI: **10.3390/polym15010182**.

51 M. G. Mohamed, M. H. Elsayed, A. E. Hassan, A. Basit, I. M. A. Mekhemer, H. H. Chou, K. H. Chen and S. W. Kuo, Hybrid Porous Polymers Combination of Octavinylsilsesquioxane/Pyrene with Benzothiadiazole Units for Robust Energy Storage and Efficient Photocatalytic Hydrogen Production from Water, *ACS Appl. Polym. Mater.*, 2024, **6**, 5945–5956, DOI: **10.1021/acsapm.4c00655**.

52 A. M. Elewa, A. F. M. EL-Mahdy, M. H. Elsayed, M. G. Mohamed, S. W. Kuo and H. H. Chou, Sulfur-doped triazine-conjugated microporous polymers for achieving the robust visible-light-driven hydrogen evolution, *Chem. Eng. J.*, 2021, **421**, 129825, DOI: **10.1016/j.cej.2021.129825**.

53 I. M. A. Mekhemer, Y. S. Wu, A. M. Elewa, W. C. Chen, C. C. Chueh and H. H. Chou, Solar-driven photocatalytic hydrogen production thiophene-quinoxaline-based polymer dots with tunable molecular weight, *Polym. J.*, 2024, **56**, 1079–1088, DOI: **10.1002/solr.202300994**.

54 I. M. A. Mekhemer, M. M. Elsenety, A. M. Elewa, K. D. G. Huynh, M. M. Samy, M. G. Mohamed, D. M. Dorrah, D. C. K. Hoang, A. F. Musa, S. W. Kuo and H. H. Chou, Push–pull–pull interactions of 2D imide–imine-based covalent organic framework to promote charge separation in

photocatalytic hydrogen production, *J. Mater. Chem. A*, 2024, **12**, 10790–10798, DOI: **10.1039/D4TA01108B**.

55 I. M. A. Mekhemer, Y. S. Wu, A. M. Elewa, W. C. Chen and C. C. Chueh, Naphthalenediimide-Based Polymer Dots with Dual Acceptors as a New Class of Photocatalysts for Photocatalytic Hydrogen Generation under Visible Light Irradiation, *Sol. RRL*, 2024, **6**, 2300994, DOI: **10.1002/solr.202300994**.

